High-temperature phase transition in the three-layered sodium cobaltite Pf3-NaxCoO2 (x 0.62)

Maxime Blangero, Dany Carlier-Larregaray, Michaël Pollet, Jacques Darriet, Claude Delmas, Jean-Pierre Doumerc

High temperature phase transition in the three-layered sodium cobaltite P'3-Na_xCoO_2 (x ~ 0.62)

Maxime Blangero, Dany Carlier, Michaël Pollet, Jacques Darriet, Claude Delmas and Jean-Pierre Doumerc

ICMCB, CNRS, Université Bordeaux 1

87 Av. du Dr. A. Schweitzer, 33608 Pessac cedex, France

Corresponding author: blangero@icmcb-bordeaux.cnrs.fr

Abstract

The high temperature phase transition in the three–layered P'3-Na_xCoO_2 (x ~ 0.62) has been investigated by means of heat capacity measurement, X-ray diffraction and ^{23}Na MAS-NMR spectroscopy in the 300–550 K range. The phase transition occurs nearby T_S = 350 K. Below T_S, the unit cell is monoclinic (Space group C2/m). Above T_S, the monoclinic cell is reversibly converted into a rhombohedral cell (Space group R3m). The crystallographic change mainly manifests into Na rearrangement in the interslab from a low symmetry position to a higher symmetry position. A global picture for both systems of the (x,y,z) off-center position of Na could be understood as a balance between onsite Na^+-$Co^{3+/4+}$ electrostatic repulsions (z-shift) and in-plane Na^+-Na^+ electrostatic repulsions (xy-shift). We suggest that Na^+ interlayer redistribution is the driving force of the phase transition. ^{23}Na MAS-NMR spectroscopy has been used to investigate changes in the environment and in the distribution of the sodium cations occurring by raising the temperature. The gradual suppression of the second order quadrupolar interactions and

the resulting new resonance is consistent with the sodium site exchange mechanism. Changes in the resistivity at T_S suggest a strong coupling between the Na^+ and CoO_2 layers.

PACS

61.05.cp, 61.66.-f, 67.80.dk, 64.60.-i, 65.40.-b

Introduction

In the 80's, Na_xCoO_2 has been widely investigated as potential electrode materials for sodium batteries in Bordeaux.[1] The same research group reported the thermodynamic phase diagram of Na_xCoO_2 and measured the unusually large thermoelectric power of 80 μV/K associated with low metallic-like electrical resistivity of 3 mΩ.cm at 300 K for polycrystalline $Na_{0.7}CoO_2$ powder.[2,3] More recently Na_xCoO_2 gained a renewed interest after the measurement of the promising thermoelectric power factor of $Na_{\sim 0.7}CoO_2$ single crystals[4] and the discovery of superconductivity in hydrated $Na_{0.35}CoO_2\ 1.3H_2O$[5].

Four thermodynamic stable phase domains have been identified depending on the alkali content[6]. All phases consist of an alternate stacking of slabs of edge-shared CoO_6 octahedra and of partially deficient alkali layers. They differ in the packing sequence of oxygen layers that leads to different oxygen environment for Na^+ ions, octahedral (O) or prismatic (P), and to a different number of CoO_2 sheets - 2 or 3 - within the pseudo-hexagonal unit cell. According to Delmas *et al.* nomenclature[7], three of them are three-layered structures and are designated by O3 for $0.9 \leq x \leq 1$, O'3 for $x = 0.75$, and P'3 for $0.55 \leq x \leq 0.68$; the prime superscript refers to a monoclinic distortion of the unit cell. Only for $x \sim 0.7$ a two-layered P2 structure with interesting thermoelectric properties is obtained.

In P'3-Na_xCoO_2, all the Na^+ ions are occupying a single type of prismatic site that on one side is sharing a face and on the other side is sharing edges with surrounding CoO_6 octahedra. This situation is very different from that of P2-Na_xCoO_2 where two distinct prismatic sites are found: one is sharing only faces whereas the second one is sharing

only edges with CoO_6 octahedra. The room temperature monoclinic distortion β of the P'3 family has been accurately determined[8,9]. The monoclinic unit cell contains a single layer and the space group is C2/m. For $x = 0.69$, the monoclinic angle β is equal to 106.05° which is slightly less than the corresponding angle of 106.52° deduced from the pseudo-hexagonal cell reported by Fouassier *et al.6*.

The physical properties of this system in the low temperature region have been widely investigated. Little is however known about the high temperature behavior of this oxide family. In this study, a high temperature phase transition from a monoclinic to a higher rhombohedral symmetry is reported and its temperature dependence is followed by means of XRD and ^{23}Na MAS-NMR. To our knowledge, this is the first ^{23}Na MAS-NMR study of the Na_xCoO_2 ($0.5 < x < 1$). Other groups studied the P2 compounds as single crystal or aligned powder with broad line type NMR spectrometers. In these studies Na^+ ions are said to be mobile from ~200-250 K.[22,23] However, we show by variable temperature ^{23}Na MAS-NMR, that Na^+ ions are not fully exchanged at room temperature and that the motion is activated upon heating. Anomalies in the temperature dependences of the specific heat and electrical resistivity are discussed regarding this phase transition.

Experimental

The synthesis of polycrystalline powder of P'3-Na_xCoO_2 ($x \approx 0.62$) has already been reported in details 6. In short, a conventional solid-state reaction route has been used: powders of Na_2O and Co_3O_4 were intimately mixed under argon in a glove box and heated for 12 h to 823 K under dry oxygen flow. Since by-produced Na_2O is highly volatile, a 10 wt% excess is added. After heating and cooling, the black product was immediately put under dry argon atmosphere to prevent moisture contamination. All the characterizations were performed on the same batch.

XRD patterns of $Na_{0.62}CoO_2$ were recorded with a Philips X'Pert Pro powder diffractometer in the Bragg-Brentano geometry, using cobalt Kα radiations. The data collections were made in the 10-120° 2θ range with a 0.0167° step, using an X'Celerator PSD detector. The powder was kept in an airtight holder under dry argon for room temperature X-ray diffraction to prevent any reaction with air moisture (Linear PSD aperture of 0.512 mm, counting time: 240 s/step). High temperature X-ray diffraction was performed in an Anton Paar HTK 1200N oven-chamber under dry oxygen flow (Linear PSD aperture of 1.019 mm, counting time: 350 s/step).

The diffraction data were analyzed using the Rietveld technique[10] as implemented in the Fullprof program.[11] Peak shape was described by a pseudo-Voigt function, and the background level was fitted with linear interpolation between a set of given points with refinable heights. The sodium content of the unit cell was set according to ICP-AES elementary determination that leads to the raw formula $Na_{0.62(2)}CoO_2$.

Single pulse ^{23}Na magic angle spinning (MAS) NMR spectra were recorded on a Bruker 300 Avance spectrometer at 79.403 MHz, with a standard 4 mm Bruker MAS probe. Polycrystalline samples were mixed with dry silica (typically in a 1:1 weight ratio), in order to facilitate the spinning and improve the field homogeneity, since they may exhibit metallic or paramagnetic properties. The mixture was placed in 4 mm diameter zirconia rotors in a dry box. No change in the NMR signal was observed even for rotors kept several days out of the dry box, indicating good air-tightness of the cell. A short pulse length of 1 μs corresponding to a selective $\pi/12$ pulse determined using an aqueous 0.1 mole/L NaCl solution was employed. A spinning speed of 13 kHz was used. The spectral width was set to 1 MHz, and the recycle time $D_0 = 0.5$ s, was long enough to avoid T_1 saturation effects with 1600 scans per spectrum. The baseline distortions resulting from the spectrometer dead time (5-10 μs) were removed computationally using a polynomial baseline correction routine. 1600 scans variable temperature (VT) NMR experiments were also carried out in the 300 K-470 K range using a Bruker WVT MAS probe. The external reference was a 0.1 mole/L NaCl aqueous solution.

Heat capacity measurements were made in a helium Quantum Design PPMS cryostat using the "2-tau relaxation method" in the 1.8-400 K range under high vacuum. Above 300 K, sample radiation losses may affect the specific heat accuracy. Sample heat capacity is calculated by carefully subtracting a blank measurement, including both the contribution of the sample platform and of the grease used to attach the sample to the puck, from the total heat capacity measurement. C_p for C_v correction has not been performed as the resulting error is assumed negligible in the explored temperature range (around 5 % for $T \sim \theta_D$).

Field cooled (FC) DC-magnetization data in an applied field of 1 T were collected on a superconducting quantum interference device magnetometer (Quantum Design) in the 2-300 K temperature range. For higher temperature ranges (*i.e.* 300-500 K), the paramagnetic susceptibility was measured on a DSM-8 stationary pendulum susceptometer of Manics Équipement Scientifique, under an applied field of 1 T. Field dependency of the magnetization was found linear down to 5 K.

Transport properties were measured on raw pellets (10 mm in diameter) pressed under 10 MPa, the compactness of which was close to 70 %. Electrical DC conductivity measurements were performed with the aligned four-probe method in the 4.2-500 K range.

Structure determination

X-ray diffraction patterns of P'3-$Na_{0.62}CoO_2$ at 300 K and 393 K are displayed in Figures 1a and 1b, respectively. As previously reported8, the room temperature XRD pattern of the as-obtained P'3-$Na_{0.62}CoO_2$ was accounted for by means of a monoclinic unit cell with space group C2/m and parameters: $a_m = 4.8996(6)$ Å, $b_m = 2.8263(2)$ Å, $c_m = 5.7156(5)$ Å and $\beta = 106.069(6)°$. Insets of Figures 1a and 1b focused on the 30-36° 2θ-range. Additional weak peaks, each of them representing about 0.6 % of the intensity of the strongest (001) peak, are observed in the monoclinic phase and reversibly disappear on heating. Figure 2 displays XRD patterns recorded from 483 K down to RT for the $32° < 2\theta < 70°$ range. Upon cooling, peak shape significantly changes and reflections such as (015), (107) and (018) are split into the monoclinic (201)/(-112), (112)/(-203) and (202)/(-113) doublets, respectively.

No indisputable evidence about any possible commensurate or incommensurate ordering of the Na^+ ions within the partially occupied sites was obtained in the present study but, withal, the reversible vanishing of these peaks above T_S can be considered as manifestations in support of it (right hand side of Figure 2).

The monoclinic cell parameters and those of the hexagonal cell corresponding to the rhombohedral phase ($\mathbf{a_h}$,$\mathbf{b_h}$,$\mathbf{c_h}$) reported by Fouassier *et al*.6 for P'3-$Na_{0.6}CoO_2$ (Space group R3m) are linked by the relationship:

$$\left(\mathbf{a_m}, \mathbf{b_m}, \mathbf{c_m}\right) = \left(\mathbf{a_h}, \mathbf{b_h}, \mathbf{c_h}\right)\begin{bmatrix} 1 & 1 & -1/3 \\ -1 & 1 & 1/3 \\ 0 & 0 & 1/3 \end{bmatrix} \quad (1)$$

The high temperature dataset was successfully fitted using the space group R3m and the rhombohedral cell proposed by Fouassier *et al*. A Rietveld refinement of the structure at 393 K has been subsequently performed using these settings. Table 1 summarizes the structural parameters for P'3- and P3-$Na_{0.62}CoO_2$ at RT and 393 K, respectively. The atomic positions of cobalt and oxygen atoms have been deduced from (1): cobalt atoms are distributed in the 3a site (0,0,0); the oxygen atoms occupy two positions, O1 and O2, both in 3a site (0,0,z) with z ~ 0.3901 and 0.6099, respectively. A difference Fourier map clearly shows that sodium atoms are only located in two equivalent positions: the first in 3a site (0,0,z) with z ~ 0.8324 and the second, also in 3a site (⅓,⅔,z) with z ~ 0.8343. The high temperature stable phase is of P3-type, *i.e.* the structure remains three-layered-like and Na^+ ions are located in trigonal prisms. A representation of both structures is given in Figure 3.

The primary difference between the high temperature and low temperature forms is that the Na^+ ions reside at a higher symmetry prism for P3 structure as compared to P'3

structure. The Na coordination polyhedra and associated Na-O distances are presented in Figure 4. In P'3, the sodium atoms occupy prismatic sites with Na-O distances ranging from 2.223 Å to 2.634 Å (Table 1). These distances are in good agreement with those generally encountered for this atom. In both structures, the Na-O distances differ whether the oxygens of the CoO_6 octahedra are sharing a face (subscript f) or an edge (subscript e) with NaO_6 prisms. Average $Na\text{-}O_f$ distances (2.448 Å in P'3-phase and 2.453 Å in P3-phase) are larger than average $Na\text{-}O_e$ distances (2.383 Å in P'3-phase and 2.430 Å in P3-phase). This result can be ascribed to a larger electrostatic repulsion for face-sharing polyhedra (shorter Na-Co distance) than for edge-sharing polyhedra (longer Na-Co distance).

In the monoclinic phase, Na^+ ions are shifted out of the (x,y) center of their prisms, while this is not the case in the rhombohedral phase. When a particular Na site is occupied, the Na-Na distance with its first-nearest-neighbor sites is too small compared to Na^+ diameter to allow simultaneous occupation. The coulombic repulsion of the Na^+ ion by Na^+ ions occupying second-nearest-neighbor Na sites should therefore dominate Na^+ arrangement within the interslab. Occupying off-centered in plane positions allow for larger Na-Na sites distances, thereby minimizing the coulombic repulsion of the Na^+ ions. The distribution of the Na-O distances clearly shows that the coulombic Na^+-Na^+ repulsion is strong enough to displace the Na^+ ions from the center of their prisms (Table 1). Similar electrostatic effects were considered to explain potassium orderings in $K_4Co_7O_{14}$[12] and the off-centered position in P2-Na_xCoO_2[13,14,15] where two distinct alkaline sites are available. In the two-layered family, the sodium forms many ordered phases with various sodium contents, both commensurate and incommensurate with the underlying CoO_2 hexagonal

slabs[16,17,40]. Direct evidences of structural phase transitions through Na ordering in Na_xCoO_2 upon cooling have also been reported[18,19,20]. Likewise, the same situation should also be reasonably expected in our system regarding the reversible vanishing of the extra reflections below and above T_S (Insets of Figures 1a and 1b), and we propose that the vanishing of the Na^+ ordering above T_S is the driving force for the phase transition.

^{23}Na MAS-NMR spectroscopy

Powder ^{23}Na MAS-NMR spectra are shown on Figure 5. The MAS-NMR technique allows averaging both the first order quadrupolar interactions and nuclear dipolar interactions, mainly responsible for the broadening of the NMR lines. At room temperature, the P'3-$Na_{0.62}CoO_2$ phase exhibits a single shifted signal located around 350 ppm with a clear second order interaction shape typical of Na^+ ions located in an asymmetric environment. A set of spinning side bands are also observed on both sides of this signal. Note that another signal located around 0 ppm is also observed and assigned to a small amount of diamagnetic sodium impurities in the sample with longer T1 relaxation time that are not seen by XRD. Its significant decrease as the temperature is raised can be ascribed to the decrease of the population of excited quantum states of the nuclei.[21] At room temperature, an averaging of the cobalt ion charges has been evidenced by ^{59}Co and ^{23}Na NMR in several two-layered Na_xCoO_2 phases.[22,23] Hence, in the P'3 and P3 phases, the sodium ions are surrounded by equivalent cobalt ions at and above room temperature.

As the temperature increases, the isotropic chemical shift of the Na NMR line is shifted to lower values denoting Fermi contact mechanism that is in good agreement with the

Curie-Weiss paramagnetic behavior of this compound. The temperature elevation also results in a gradual collapse of the second-order quadrupolar line shape and to the emergence of a narrower central resonance. The vanishing of the second-order quadrupolar contribution is expected for a ^{23}Na ion in highly symmetric environment with weak or no electric field gradient (EFG).

Upon cooling, exactly opposite effects are observed and the spectra recorded at room temperature at the end of the experiment is similar to the first one (Fig. 5), indicating a good reversibility of the phenomenon.

In the monoclinic P'3-$Na_{0.62}CoO_2$ sample at room temperature (Fig. 4), sodium ions occupy crystallographic positions that are shifted out of the center of their prisms. This asymmetric oxygen environment of Na is likely to result in strong quadrupolar interactions. Possible Na distribution resulting from the Na/vacancy ordering could account for the relatively broad lineshape of this second-order quadrupolar signal. As the temperature increases, the gradual disappearance of the 2nd order lineshape and the emergence of a narrower central resonance without quadrupolar second-order shape are resulting from the motion of the sodium cations in the interslab space at the timescale of NMR spectroscopy. Previous ^{23}Na NMR studies on the two-layered $Na_{0.7}CoO_2$ also evidenced Na^+ ion motion above $T = 250$ K23. Ionic conductance of these lamellar oxides is known for long time in the scope of sodium batteries1,24. The Na^+ ion's motion pathway between oxygen layers occurring in the tree-layered system is depicted in Figure 6. Na^+ ions migrate only through the faces of the prisms. The bottleneck radius for sodium in the P'3 and P3 systems are calculated to be 0.860 Å and 0.901 Å, respectively. According to Shannon's radii tables, Na^+ ionic radius in a six-fold polyhedron is

estimated to be 1.02 Å. This suggests that Na^+ ions can move freely through this material as there are tunnels available for motion between the oxygen layers, even at room-temperature[25]. Two adjacent Na prismatic sites are equivalent in the (*ab*)-plane but opposite along the *c*-direction, which is the main direction of the EFG, resulting in opposite V_{zz} electric field gradient. The mobility of the sodium cations in this phase thus results, by exchange phenomenon, in a cancellation of the V_{zz} contribution and therefore in a signal narrowing and a suppression of the 2nd order quadrupolar effect. The averaged signal at NMR timescale is therefore similar to the one expected for a single Na^+ ion in a highly symmetric environment. For comparison and as preliminary results, we also studied by ^{23}Na MAS NMR the P2-$Na_{0.6}CoO_2$ phase, where the adjacent Na sites are not equivalent regarding the Co environment and the V_{zz} EFG contribution can therefore not be suppressed. In that case, the sodium ions mobility leads to a narrowing of the signal keeping a clear the 2nd order quadrupolar interaction shape in all the temperature range (300 K to 470 K). These results will be published elsewhere[26].

The P'3-P3 phase transition do not correspond to an abrupt change in the ^{23}Na signal, but to a progressive modification from a 2nd order line shape to a symmetric site line shape. This progressive evolution is also true in the P'3 phase; therefore the Na mobility increases when temperature increases leading to a progressive cancellation of the V_{zz} main EFG term, as well.

In this picture, the collapse of the second-order quadrupolar lineshape and the new resonance observed when the temperature increases mainly originates from fast chemical exchange between sodium sites that is sufficiently fast to average quadrupolar

interactions at ^{23}Na MAS-NMR timescale. These observations are in line with other ^{23}Na MAS-NMR characterizations on zeolites[27].

Specific heat measurements

Figure 7a shows the specific heat capacity C_p of the tree-layered $Na_{\sim 0.62}CoO_2$ phase from 1.8 K to 400 K. Over the 1.8 – 270 K temperature range the data cannot be fitted using a single Debye model. A better picture of the specific heat was achieved considering both an electronic contribution and two Debye contributions:[28]

$$C_p(T) = \gamma_{HT} T + 9R \sum_{i=1}^{2} n_i \left(\frac{T}{\theta_i}\right)^3 \int_0^{\theta_i/T} \frac{x^4 e^x}{\left(e^x - 1\right)^2} dx \quad (2)$$

The first term $\gamma_{HT}T$ represents the temperature-linear electronic contribution and the second term is the Debye-type contribution (two acoustic modes). R = 8.314 J/mole K is the molar gas constant, θ_i are the Debye temperatures and n_i are the number of atoms per mole of $Na_{0.62}CoO_2$ for each Debye mode. The large differences in the bond character between Co-O (covalent-like) and Na-O (ionic-like) and the relatively large mobility of Na^+ ions in the interslab justify the use of two different phonon spectra, each of them being associated to a (θ_i, n_i) couple (i = 1,2). A decent agreement with the dataset was achieved with $\gamma_{HT} = 23.0(1) \times 10^{-3}$ J/mole K^2, $\theta_1 = 291(1)$ K and $\theta_2 = 855(1)$ K, n_1 (Na^+ contribution) and n_2 (CoO_2 contribution) being constrained to 0.62 and 3, respectively. θ_2 (CoO_2) > θ_1 (Na^+) is also in good agreement with the highest Co-O bond stiffness compared to Na-O. The Co^{3+}-O bond is very covalent and the covalency increases with the cobalt oxidation state and, as a consequence, a very stiff CoO_2 sub-lattice is expected for Na_xCoO_2 as x decreases. The large θ_2 value is supported by our studies of the

pristine-like $LiCoO_2$ ($\theta_D \sim 800$ K)[29] and available data in the literature for oxides such as Al_2O_3 ($\theta_D \approx 950$ K)[30], rutile and anatase TiO_2 ($\theta_D \approx 940$ K)[31,32], GeO_2 ($\theta_D \approx 780$ K)[33] and VO_2 ($\theta_D \approx 760$ K)[34].

At high temperature, a broad peak ranging from 290 K to 355 K is observed and its maximum is estimated at around $T_S = 350$ K. This transition is attributed to the space rearrangement of Na^+ ions within the network. Similar rearrangement of sodium has been reported in the P2-$Na_{0.7}CoO_2$ system, where a large fraction of sodium ions are shifted from a high symmetry 2c (⅔,⅓,¼) site to a lower symmetry 6h (2x,x,¼) site[35]. The measured entropy change at the transition is ~0.7 J/mole K. This relatively small value is close to that reported for a P2 phase with nearly the same sodium rate.36 A quantitative discussion of the entropy change value at T_S is beyond the scope of this study as it's determination should be based on a more accurate subtraction of background and take into account the previously mentioned sample radiation losses.

At temperatures below 10 K, the electronic contribution to the specific heat has been calculated using the Debye model. A linear fit to the data using $C/T = \gamma + \beta T^2$ equation (inset of figure 7a) gives $\gamma = 26.1(1) \times 10^{-3}$ J/mole K^2 and $\beta = 3.92(5) \times 10^{-5}$ J/mole K^4. The overall θ_D value of 562 K deduced from $\beta = 12\pi^4(n_1+n_2)R/(5\theta_D^3)$ is in line with previous estimates[36,49] and is fairly close to the weighted Debye temperature deduced from (2) and calculated to be 494 K. The γ value is very close to γ_{HT} obtained from (2) and is about an order of magnitude larger than that of usual metals. The large γ value is consistent with the metallic-like character and denotes large electronic correlations. The good agreement between both low and high temperature models indicates that no additional magnetic phenomenon are occurring at low temperature.

Magnetic and electric measurements

The magnetic molar susceptibility for $Na_{0.62}CoO_2$ is given in Figure 7b. Following previous reports, the data were fitted in the investigated range using a Curie-Weiss law including a temperature independent term χ_0: $\chi(T) = \chi_0 + C/(T-\theta_p)$, with $\theta_p = -142(3)$ K, $\chi_0 = 276(5)\times10^{-6}$ cm^3/mole and $C = 0.145(2)$ cm^3 K/mole. A small deviation from the Curie-Weiss law is observed below 30 K, but its origin is unknown.

The negative θ_p value denotes antiferromagnetic interactions between spin carriers. The Curie constant (C) agrees with a (S = ½) spin concentration (or a formal atomic content of low spin Co^{4+}) of 39 % ($\mu_{eff} = 1.08\ \mu_B$) in good agreement with the nominal composition. This behavior has been previously ascribed to full spin polarization of itinerant carriers[37]. The coexistence of a large χ_0 with a Curie-Weiss contribution is unexpected. The large positive χ_0 value cannot solely be explained by a second order orbital (Van Vleck) contribution of low spin Co^{3+} closed 3d-shells estimated to ~150×10^{-6} cm^3/mole and partially balanced by a diamagnetic contribution (~-50×10^{-6} cm^3/ mole).[38,39]

In recent studies, partial (S = ½) Co^{4+} hole localization has been suggested, which could account for the antiferromagnetic interactions.[40,41,42,43,44,45,46] In such a case, localized moments accounting for the Curie-Weiss term could coexist with itinerant carriers accounting for a large χ_0. Clearly, the magnetic properties of these metallic cobaltites for which, depending on the alkali rate x, the magnetic behavior changes from Pauli type ($x < 0.5$) to Curie-Weiss type ($x > 0.5$) are still not fully understood.[47] In the case of Pauli

type Na_xCoO_2 ($x < 0.5$)47 or in potassium homologues ($x = 0.6$)[48,12], the Pauli susceptibility value is strongly enhanced, by the electronic correlations.

No magnetic transition is observed at T_S, which is substantially different from what has been reported in the two-layered system for which weak changes in χ (about 1 %) where measured at the temperature of sodium rearrangement.35,[49]

The resistivity at high temperature and upon cooling is reported on Figure 7c. A steep departure from the low temperature metallic regime is observed at 297 K, and then a sharp decrease of ρ occurs up to 360 K, which is followed by another metallic regime. This high temperature feature is associated with the structural transition which is mainly affecting Na ion sites and the interslab distance. The latter change can be understood as an increase of the 2D character with the increase of temperature: the average in-plane Co-Co distances in the P'3 and P3 phases are almost identical and equal to ~2.8275 Å, whereas expansion of the *c*-axis leads to a noticeable increase in the NaO_2 interslab distance, from 3.526 to 3.630 Å. Simultaneously, the CoO_2 slab thickness decreases from 1.967 to 1.876 Å. In Na_xCoO_2, the *c*-axis increases with decreasing x resulting in a largest compression of the CoO_6 octahedron and an increase of metallicity. The D_{3d} distortion of CoO_6 octahedron lifts the degeneracy of the three-fold t_{2g} orbitals into one a_{1g} singlet and one e_g' doublet. Both *ab initio* calculations[50] and experimental works[51,52] provide evidence that the e_g' doublet is stabilized by the D_{3d} distortion. Likewise, this structural change that increases the compression of the CoO_6 octahedra along the *c*-axis may modify the spatial distribution of the a_{1g} and e_g' orbitals and therefore may affect the transport properties.

On the other hand, the sodium distribution in the interslab may also play a role. The ionic contribution of Na^+ ions to the electrical conductivity is much lower than the electronic

conductivity and its vanishing through the freezing of the Na^+ ions could not account for the sharp increase of ρ at 297 K, upon cooling. Strong correlations between the Na^+ ions and the charge carriers, that are (S = ½) holes hopping in a diamagnetic background of Co^{3+} ions are leading to an insulating state at low temperature for x = ½.47 For x > 0.5, the effects are expected to remain and the carriers are still influenced by the patterning of Na ions and modulations of the Madelung's potential in the interlayers resulting in charge localization.40,41,45 The freezing of Na^+ atoms could result in the sharp increase in ρ giving rise to a metal-metal transition in our compound. The localization effect is also expected to be enhanced in the three-layered system as each NaO_6 prisms are sharing a face with one of the surrounding CoO_6 octahedra. Former reports on the two-layered P2 system are further divided into two series: those (in line with this work) characterized by a sharp increase in the resistivity18,36,53,54 and those (contrasting with this work) showing a sharp drop in resistivity35,49. Hysteretic and partially irreversible behavior in the transport properties has been reported in P2 phases[55]. Our measurements of the resistivity upon heating (not shown) and cooling show the same anomalies and will be discussed in detail elsewhere. Further work is needed to assess whether charge localization linked to sodium patterning or the increase in the 2D-character is the dominant effect in the electronic behavior at the phase transition.

Acknowledgements

This work was financially supported by the Council of Région Aquitaine, Centre National de la Recherche Scientifique (CNRS) and the French National Research Agency (ANR). M. Ménétrier, E. Bekaert and M. Pouchard (ICMCB-CNRS) are deeply acknowledged for fruitful discussions. The authors also thank Cathy Denage (ICMCB-CNRS) who provided experimental backup and R. Decourt (ICMCB-CNRS) for technical assistance in transport measurements.

Tables

Table I. Structural parameters for the monoclinic P'3-$Na_{0.62}CoO_2$ at room temperature and the rhombohedral P3-$Na_{0.62}CoO_2$ at 393 K.

	P'3-$Na_{0.62}CoO_2$ at 300 K	P3-$Na_{0.62}CoO_2$ at 393 K	
Space group	C2/m (Z = 2)	R3m (Z = 3)	
Lattice Parameters			
a (Å)	4.8995(6)	2.8276(2)	
b (Å)	2.8263(2)	2.8276(2)	
c (Å)	5.7155(5)	16.518(3)	
β (°)	106.069(6)	*106.515(6)**	
Atomic Positions			
	Na	**Na1**	**Na2**
Sites	*8j*	*3a*	*3a*
(x,y,z)	(0.820(2),0.098(5),0.492(1))	(0,0,0.8324(3))	(⅓,⅔,0.8343(3))
Occ.	0.155	0.31	= Occ.(Na1)
U ($Å^2$)	0.0076(13)	0.030(3)	= U(Na1)
	Co	**Co**	
Site	*2a*	*3a*	
(x,y,z)	(0,0,0)	(0,0,0)	
Occ.	1	1	
U ($Å^2$)	0.009(4)	0.008(4)	
	O	**O1**	**O2**
Sites	*4i*	*3a*	*3a*
(x,y,z)	(0.3892(6),0,0.1791(4))	(0,0,0.3901(6))	(0,0,0.6099(6))
Occ.	1	1	1
U ($Å^2$)	0.0076(6)	0.014(4)	= U(O1)
Selected Distances			
Na-O_e (Å)	1×2.223(10) 1×2.375(12) 1×2.551(11)	3×2.430(8)	
Na-O_f (Å)	1×2.318(11) 1×2.393(10) 1×2.634(12)	3×2.453(8)	
Co-O (Å)	2×1.898(6) 4×1.910(3)	6×1.883(5)	
CoO_2 slab thickness (Å)	1.967	1.876	
NaO_2 Interslab thickness (Å)	3.526	3.630	
Conventional Reliability Factors			
cR_{wp} (%)	11.1	12.2	
R_{Bragg} (%)	5.71	5.50	
Goodness of Fit χ^2	2.99	2.49	

*: Pseudo-β corresponding to the monoclinic cell for comparison purposes only.

Figure Captions

FIG. 1. (Color online) Rietveld refinement of powder XRD pattern of a) P'3-$Na_{0.62}CoO_2$ at 300 K and b) P3-$Na_{0.62}CoO_2$ at 393 K. The observed (crosses), calculated (solid line) and difference (bottom line) profiles as well as Bragg positions (vertical bars) are shown. The 90-120° 2θ-range is not displayed for clarity. The insets on both graphs emphasize additional peaks that appear upon cooling and that are not accounted for with the monoclinic cell.

FIG. 2. (Color online) Temperature dependence of XRD patterns of $Na_{0.62}CoO_2$ during cooling for a selected 2θ-range showing that the rhombohedral P3-phase becomes stable above 350 K. Reversible vanishing above T_S of additional reflections nearby 33° is attributed to Na^+ ordering within the interlayer.

FIG. 3. (Color online) (a) Projection along the b_m-axis of the crystal structure relationships between the low temperature monoclinic P'3 phase and the high temperature rhombohedral P3 phase. Na atoms are not shown for clarity. (b) Projection of the structure along the c_h-axis on the Co triangular array (z = 0) showing the in-plane vectors (a_h,b_h) and (a_m,b_m) and projection of the c_m-axis (short dashes).

FIG. 4. (Color online) NaO_6 prismatic environments for both P'3 and P3 phases. The "f" and "e" subscripts label oxygen atoms belonging either to a face or to an edge shared by a CoO_6 octahedron with a NaO_6 prism, respectively. The filled triangles show the CoO_6 octahedron faces that are shared with NaO_6 prisms. All distances are in angstroms.

FIG. 5. (Color online) Temperature dependence of ^{23}Na MAS-NMR spectra for P'3-$Na_{0.62}CoO_2$.

FIG. 6. (Color online) Motion scenario of Na^+ in the interslab. The filled triangles show the CoO_6 octahedron faces that are shared with NaO_6 prisms. The on-site electrical field gradient is schematized by an arrow parallel to the *c*-axis and it is antiparallel for two Na adjacent sites.

FIG. 7. (Color online) a) Temperature dependence of the specific heat (open circles), the fit using Eq. 2) (solid line) and the low temperature Debye fit (inset); b) Temperature dependence of the molar magnetic susceptibility for $Na_{0.62}CoO_2$ (open circles) and the Curie-Weiss fit (solid line), and, c) temperature dependence of the electrical resistivity (open circles). Vertical dotted lines are guide to the eyes and are demarcating the transition domain.

Figures

Figure 1

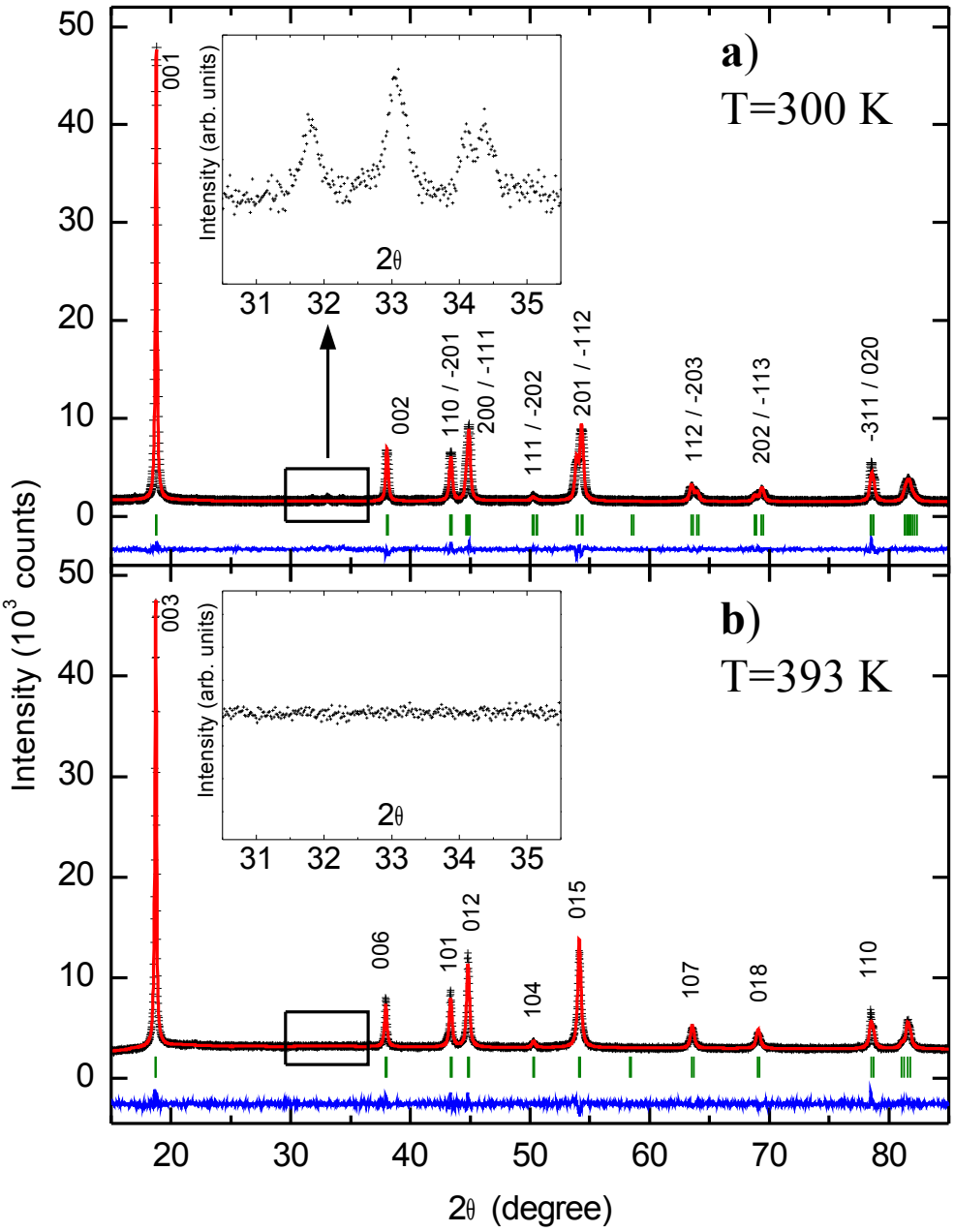

Figure 2

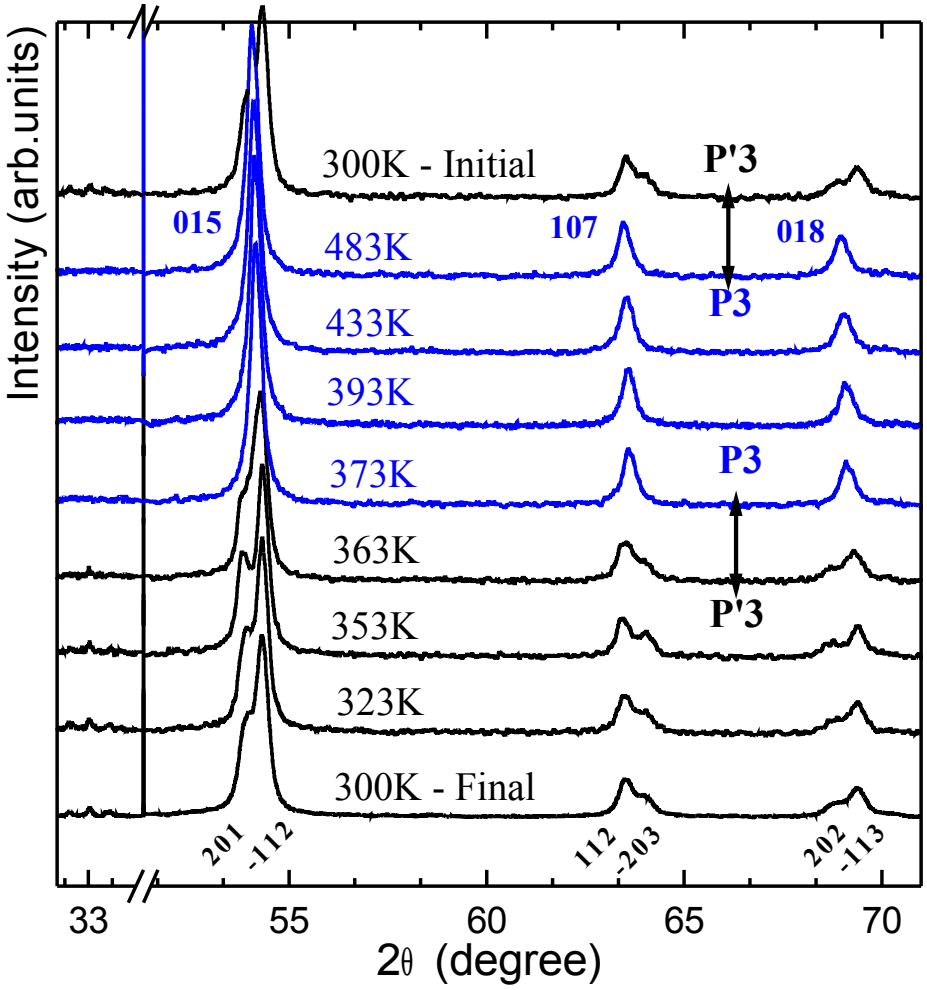
Intensity (arb.units)
300K - Initial
483K
433K
393K
373K
363K
353K
323K
300K - Final
P'3
P3
P3
P'3
015
107
018
201
-112
112
-203
202
-113
33
55
60
65
70
2θ (degree)

Figure 3

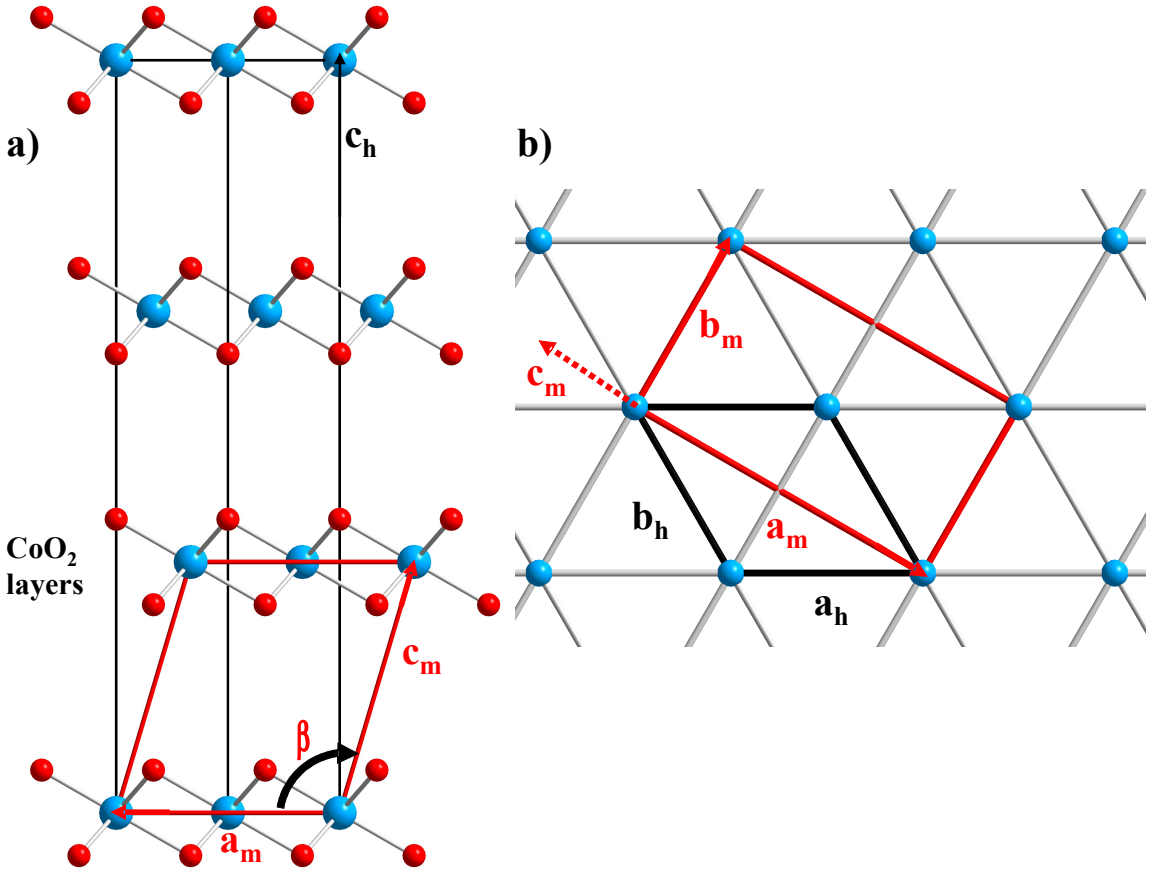

Figure 4

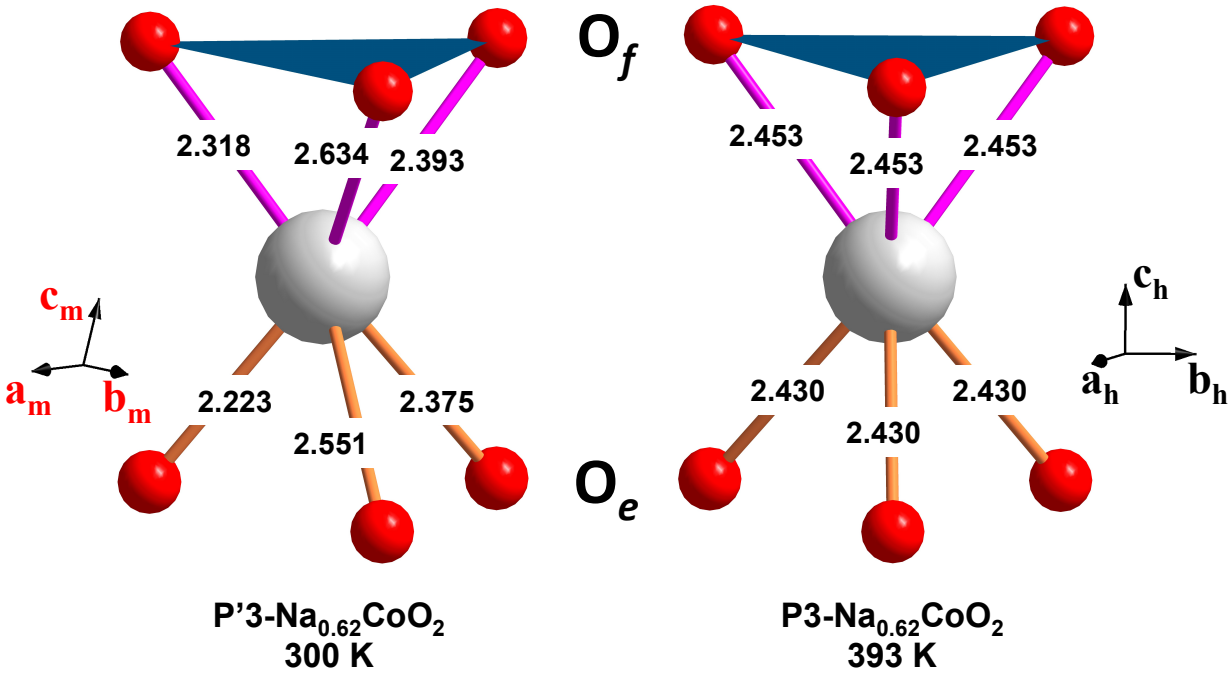
O_f
O_e
2.318
2.634
2.393
2.223
2.375
2.551
2.453
2.453
2.453
2.430
2.430
2.430
c_m
a_m
b_m
c_h
a_h
b_h
P'3-Na0.62CoO2
300 K
P3-Na0.62CoO2
393 K

Figure 5

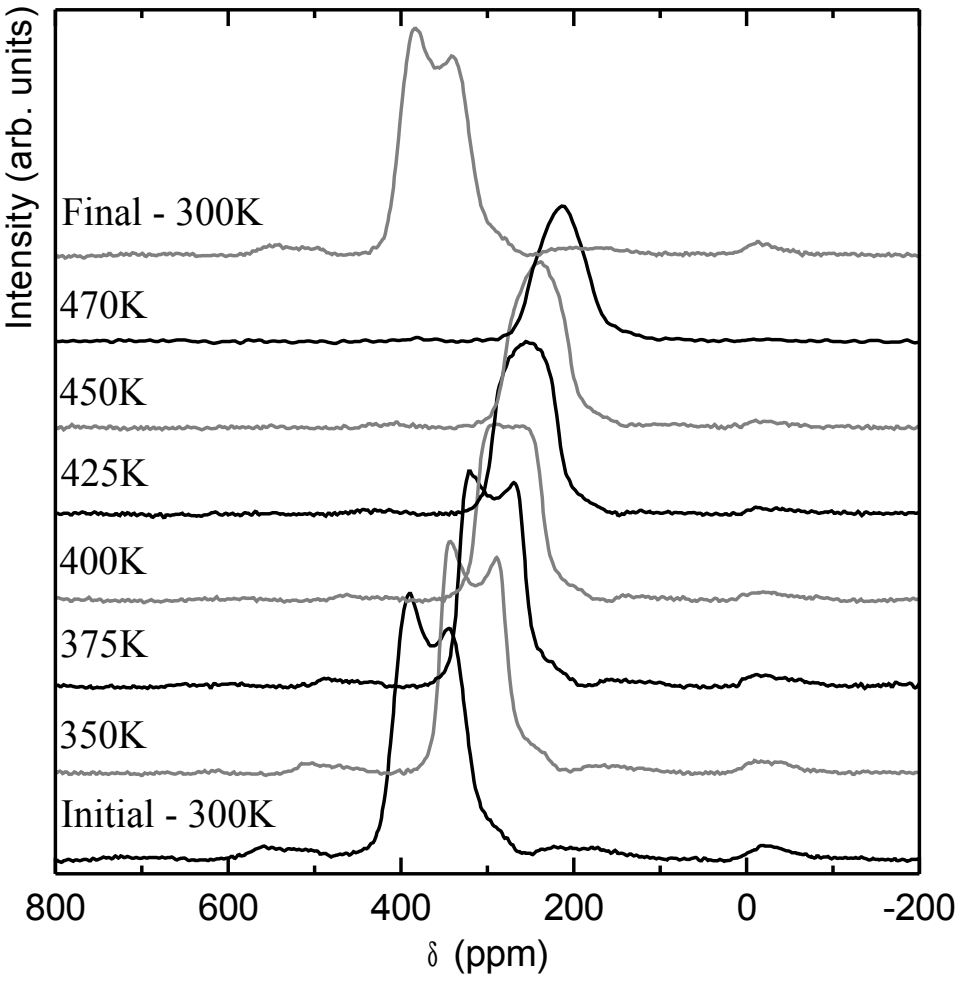
Intensity (arb. units)
Final - 300K
470K
450K
425K
400K
375K
350K
Initial - 300K
800
600
400
200
0
-200
δ (ppm)

Figure 6

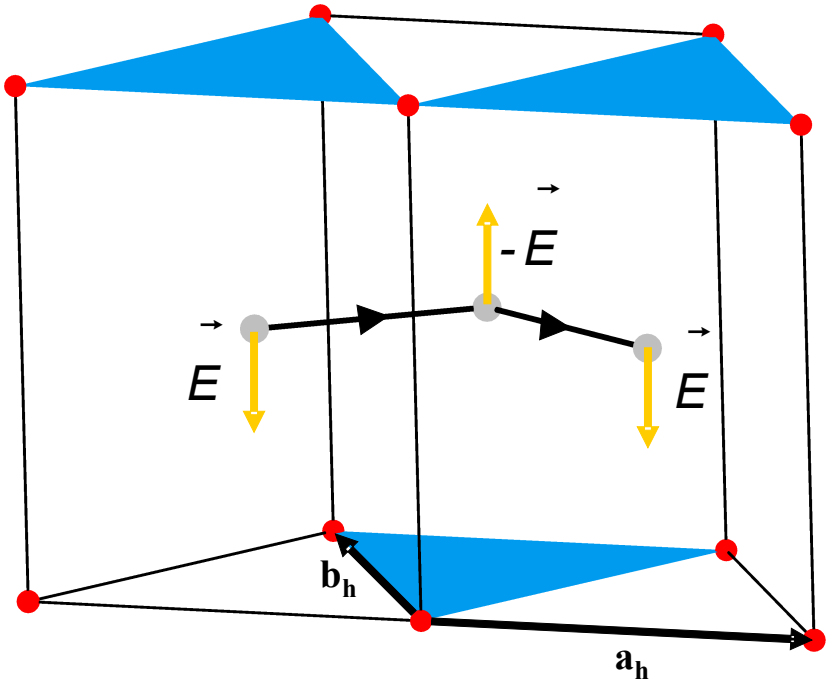

Figure 7

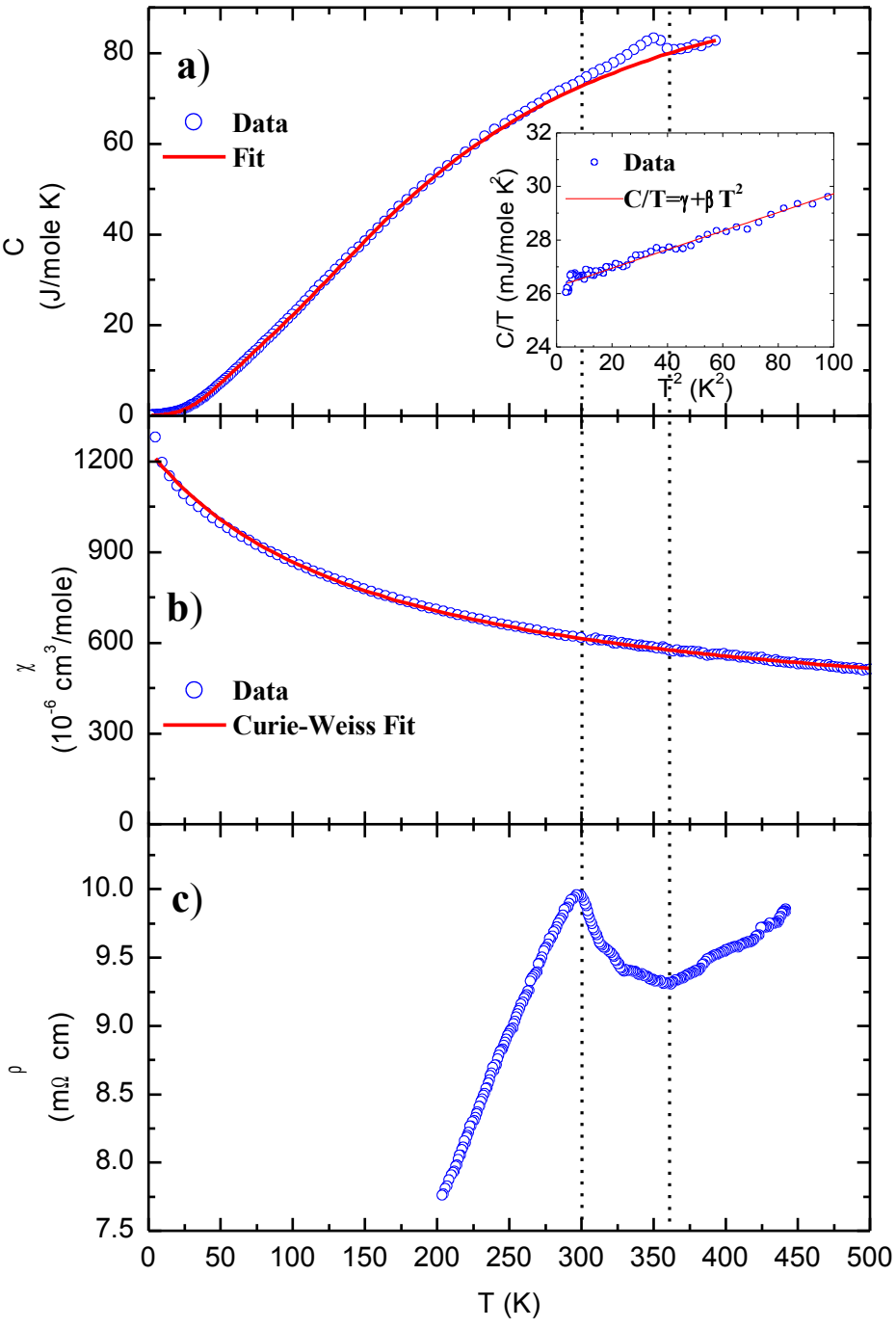
a)
Data
Fit
C
(J/mole K)
Data
C/T=γ+β T²
C/T (mJ/mole K²)
T⁻² (K⁻²)
b)
Data
Curie-Weiss Fit
χ
(10⁻⁶ cm³/mole)
c)
ρ
(mΩ cm)
T (K)

References

[1] C. Delmas, J.J. Braconnier, C. Fouassier, and P. Hagenmuller, Solid State Ionics **3-4**, 165 (1981).

[2] J. Molenda, C. Delmas, and P. Hagenmuller, Solid State Ionics **9-10**, 431, (1983).

[3] J. Molenda, C. Delmas, and P. Dordor, Solid State Ionics **12**, 473 (1984).

[4] I. Terasaki, Y. Sasago, and K. Uchinokura, Phys. Rev. B **56**, 12685 (1997).

[5] K. Takada, H. Sakurai, E.T. Muromachi, I. Izumi, R.A. Dilanian, and T.A. Sasaki, Lett. Nat. **422**, 53 (2004).

[6] C. Fouassier, G. Matejka, J.M. Reau, and P. Hagenmuller, J. Solid State Chem. **6**, 532 (1973).

[7] C. Fouassier, C. Delmas, and P. Hagenmuller, Mater. Res. Bull. **10**, 443 (1975).

[8] Y. Ono, R. Ishikawa, Y. Miyazaki, Y. Ishii, Y. Morii, and T. Kajitani, J. Solid State Chem. **166**, 177 (2002).

[9] L. Viciu, J.W.G. Bos, H.W. Zandbergen, Q. Huang, M.L. Foo, S. Ishiwata, A.P. Ramirez, M. Lee, N.P. Ong, and R.J. Cava, Phys. Rev. B **73**, 174104 (2006).

[10] H. M. Rietveld, J. Appl. Cryst. **2**, 65 (1969).

[11] J. Rodriguez-Carvajal, Physica B **192**, 55 (1993).

[12] M. Blangero, R. Decourt, D. Carlier, G. Ceder, M. Pollet, J.P. Doumerc, J. Darriet, and C. Delmas, Inorg. Chem. **44**, 9299 (2005).

[13] Q. Huang, M.L. Foo, R.A. Pascal, Jr., J.W. Lynn, B.H. Toby, Tao He, H.W. Zandbergen, and R.J. Cava, Phys. Rev. B **70**, 184110 (2004).

[14] L. Viciu, Q. Huang, and R.J. Cava, *Phys. Rev. B* **73**, 212107 (2006).

[15] J.D. Jorgensen, M. Avdeev, D.G. Hinks, J.C. Burley, and S. Short, Phys. Rev. B **68**, 214517 (2003).

[16] H.W. Zandbergen, M. Foo, Q. Xu, V. Kumar, and R.J. Cava, Phys. Rev. B **70**, 24101 (2004).

[17] Y.S. Meng, Y. Hinuma, and G. Ceder, J. Chem. Phys. **128**, 104708 (2008).

[18] Y. Shi, H.C. Yu, C.J. Nie, and J.Q. Li arXiv:cond-mat/0401052v1.

[19] H.X. Yang, C.J. Nie, Y.G. Shi, H.C. Yu, S. Ding, Y.L. Liu, D. Wu, N.L. Wang, and J.Q. Li. Solid State Comm. **134**, 403 (2005).

[20] D. Igarashi, Y. Miyazaki, K. Yubuta, and T. Kajitani, Jpn. J. Appl. Phys. **46**, 304 (2007).

[21] J.D. Roberts in *Nuclear magnetic resonance*, McGraw-Hill, (New-York), 1959.

[22] I.R. Mukhamedshin, H. Alloul, G. Collin, and N. Blanchard, Phys. Rev. Lett. **93**, 167601 (2004).

[23] J.L. Gavilano, D. Rau, B. Pedrini, J. Hinderer, H.R. Ott, S. M. Kazakov, and J. Karpinski; Phys. Rev. B **69**, 100404 (2004).

[24] C. Delmas, A. Maazaz, C. Fouassier, J.M. Réau, and P. Hagenmuller, Mat. Res. Bull. **14**, 329 (1979).

[25] R.J. Balsys and R.L. Davis, Solid State Ion. **93**, 279 (1996).

[26] D. Carlier, M. Blangero, M. Ménétrier, M. Pollet, J.P. Doumerc, and C. Delmas (unpublished).

[27] K.H. Lim and C.P. Grey, J. Am. Chem. Soc. **122**, 9768 (2000).

[28] N.W. Ashcroft and N.D. Mermin, in *Solid State Physics*, edited by Dorothy Garbose Crane (Holt, Rinehart and Winston, New York, 1976), Chap. 21, p.459.

[29] M. Ménétrier, D. Carlier, M. Blangero, and C. Delmas, Electrochemical and Solid State Letters *Submitted* (2008).

[30] L. Braginsky, V. Shklover, H. Hofmann, and P. Bowen, Phys. Rev. B **70**, 134201 (2004).

[31] T.R. Sandin, and P.H. Keesom, Phys. Rev. **177**, 1370 (1969).

[32] V. Dallacasa, Physica C **437-438**, 57 (2006).

[33] A.Y. Wu, and R.J. Sladek, Phys. Rev. B **25**, 5230 (1982).

[34] D.B. McWhan, M. Marezio, J.P. Remeika, and P.D. Dernier, Phys. Rev. B **10**, 490 (1974).

[35] Q. Huang, B. Khaykovich, F.C. Chou, J.H. Cho, J.W. Lynn, and Y.S. Lee, Phys. Rev. B **70**, 134115 (2004).

[36] J. Wooldridge, D.M^{c}.K. Paul, G. Balakrishnan, and M.R. Lees, J. Phys. Condens. Matter **17**, 707 (2005).

[37] Y. Wang, N.S. Rogado, R.J. Cava, and N.P. Ong, Nature **432**, 425 (2003).

[38] G. Lang, J. Bobroff, H. Alloul, P. Mendels, N. Blanchard, and G. Collin, Phys. Rev. B **72**, 94404 (2005).

[39] F.E. Mabbs and D.J. Machin in *Magnetism and Transition Metal Complexes*, Chapman Hall, London, (1973).

[40] M. Roger, D.J.P Morris, D.A. Tennant, M.J. Gutmann, J.P. Goff, J.U. Hoffmann, R. Feyerherm, E. Dudzik, D. Prabhakaran, A.T. Boothroyd, N. Shannon, B. Lake, and P.P. Deen, Nature **445**, 631 (2007).

[41] C.A. Marianetti and G. Kotliar, Phys. Rev. Lett. **98**, 176405 (2007).

[42] L. Balicas, Y.J. Jo, G.J. Shu, F.C. Chou, and P.A. Lee, Phys. Rev. Lett. **100**, 126405 (2008).

[43] F.C. Chou, M.W. Chu, G.J. Shu, F.T. Huang, W.W. Pai, H.S. Sheu, T. Imai, F. L. Ning, and P.A. Lee, *arXiv:0709.0085v1 [cond-mat.str-el]*, (2007). I.R. Mukhamedshin, H. Alloul, G. Collin, and N. Blanchard, *arXiv:0703.561v1 [cond-mat.str-el]*, (2007). D.J.P. Morris, M. Roger, M.J. Gutmann, J.P. Goff, D.A. Tennant, D. Prabhakaran, A.T. Boothroyd, E. Dudzik, R. Feyerherm, J.U. Hoffmann, and K. Kiefer, *arXiv:0803.1312v2 [cond-mat.str-el]*, (2008).

[44] G.J. Shu, A. Prodi, S.Y. Chu, Y.S. Lee, H.S. Sheu, and F.C. Chou, Phys. Rev. B **76**, 184115 (2007).

[45] M.H. Julien, C. de Vaulx, H. Mayaffre, C. Berthier, M. Horvatic, V. Simonet, J. Wooldridge, G. Balakrishnan, M.R. Lees, D.P. Chen, C.T. Lin, and P. Lejay, Phys. Rev. Lett. **100**, 96405 (2008).

[46] H. Alloul, I.R. Mukhamedshin, G. Collin, and N. Blanchard, EPL **82**, 17002 (2008).

[47] M.L. Foo, Y. Wang, S. Watauchi, H.W. Zandbergen, T. He, R.J. Cava, and N.P. Ong, Phys. Rev. Lett. **92**, 247001 (2001).

[48] J. Sugiyama, Y. Ikedo, P.L. Russo, H. Nozaki, K. Mukai, D. Andreica, A. Amato, M. Blangero, and C. Delmas, Phys. Rev. B 76, 104412 (2007).

[49] B.C. Sales, R. Jin, K.A. Affholter, P. Khalifah, G.M. Veith, and D. Mandrus, Phys. Rev. B **70**, 174419 (2004).

[50] S. Landron and M.B. Lepetit, Phys. Rev. B **74**, 184507 (2006), *ibid.* Phys. Rev. B **77**, 125106 (2008).

[51] M. Pollet, J.P. Doumerc, E. Guilmeau, D. Grebille, J.F. Fagnard, and R. Cloots, J. Appl. Phys. **101**, 83708 (2007).

[52] D. Qian, L. Wray, D. Hsieh, L. Viciu, R.J. Cava, J.L. Luo, D. Wu, N.L. Wang, and M.Z. Hasan, *Phys. Rev. Lett.* **97**, 186405 (2006).

[53] M. Mikami, M. Yoshimura, Y. Mori, T. Sasaki, R. Funahashi, and M. Shikano Japan. J. Appl. Phys. **42**, 7383 (2003).

[54] T. Motohashi, E. Naujalis, R. Ueda, K. Isawa, M. Karppinen, and H. Yamauchi Appl. Phys. Lett **79**, 1480 (2001).

[55] T. Ikeda and M. Onoda, J. Phys. Condens. Matter **18**, 8673 (2006).